Light-Harvesting and Photocurrent Generation by Gold Electrodes Modified with Mixed Self-Assembled Monolayers of Boron−Dipyrrin and Ferrocene−Porphyrin−Fullerene Triad

Hiroshi Imahori,* Hiroyuki Norieda,‡ Hiroko Yamada, Yoshinobu Nishimura,† Iwao Yamazaki,*,† Yoshiteru Sakata,‡ and Shunichi Fukuzumi*

Contribution from the Department of Material and Life Science, Graduate School of Engineering, Osaka University, CREST, Japan Science and Technology Corporation, Suita, Osaka 565-0871, Japan, Department of Molecular Chemistry, Graduate School of Engineering, Hokkaido University, Sapporo 060-8628, Japan, and The Institute of Scientific and Industrial Research, Osaka University, 8-1 Mihoga-oka, Ibaraki, Osaka 567-0047, Japan

Received June 16, 2000. Revised Manuscript Received October 30, 2000

Abstract: Three different kinds of mixed self-assembled monolayers have been prepared to mimic photosynthetic energy and electron transfer on a gold surface. Pyrene and boron−dipyrrin were chosen as a light-harvesting model. The mixed self-assembled monolayers of pyrene (or boron−dipyrrin) and porphyrin (energy acceptor model) reveal photoinduced singlet−singlet energy transfer from the pyrene (or boron−dipyrrin) to the porphyrin on the gold surface. The boron−dipyrrin has also been combined with a reaction center model, ferrocene−porphyrin−fullerene triad, to construct integrated artificial photosynthetic assemblies on a gold electrode using mixed monolayers of the respective self-assembled unit. The mixed self-assembled monolayers on the gold electrode have established a cascade of photoinduced energy transfer and multistep electron transfer, leading to the production of photocurrent output with the highest quantum yield (50 ± 8%, based on the adsorbed photons) ever reported for photocurrent generation at monolayer-modified metal electrodes and across artificial membranes using donor−acceptor linked molecules. The incident photon-to-current efficiency (IPCE) of the photoelectrochemical cell at 510 and 430 nm was determined as 0.6% and 1.6%, respectively. Thus, the present system provides the first example of an artificial photosynthetic system, which not only mimics light-harvesting and charge separation processes in photosynthesis but also acts as an efficient light-to-current converter in molecular devices.

A final goal in supramolecular chemistry involves molecular assemblies which allow us to develop molecular devices.[1] Photosynthesis is one of the most elegant natural molecular devices in which all of the functional components are well-organized, with the help of a protein matrix. Photosynthetic membranes include both the light-harvesting complex and the reaction center complex, which are coupled to capture solar energy and convert it into chemical energy.[2] Photoinduced energy transfer (EN) and electron transfer (ET) have so far been studied extensively using donor−acceptor linked molecules or equivalents.[3−7] It is essential to construct appropriate assembly of these molecules to convert the resulting charge-separated state into chemical or electrical energy in macroscopic quantities.[8−13] However, conventional methodologies for constructing assemblies such as Langmuir Blodgett films and lipid bilayer membranes have disadvantages for outputting the energy in terms of stability, uniformity, and manipulation, which have

* To whom correspondence should be addressed. E-mail: imahori@ap.chem.eng.osaka-u.ac.jp; yamiw@eng.hokudai.ac.jp; fukuzumi@ap.chem.eng.osaka-u.ac.jp.

† Hokkaido University.

‡ Osaka University.

(1) (a) *Molecular Electronics*; Jortner, J., Ratner, M., Eds.; Blackwell: London, 1997. (b) Lehn, J.-M. *Supramolecular Chemistry*; VCH: Weinheim, 1995.

(2) (a) *Anoxygenic Photosynthetic Bacteria*; Blankenship, R. E., Madigan, M. T., Bauer, C. E., Eds.; Kluwer Academic Publishers: Dordrecht, 1995. (b) *The Photosynthetic Reaction Center*; Deisenhofer, J., Norris, J. R., Eds.; Academic Press: San Diego, 1993. (c) McDermott, G.; Prince, S. M.; Freer, A. A.; Hawthornthwaite-Lawless, A. M.; Papiz, M. Z.; Cogdell, R. J.; Isaacs, N. W. *Nature* **1995**, *374*, 517.

(3) (a) Gust, D.; Moore, T. A.; Moore, A. L. *Acc. Chem. Res.* **1993**, *26*, 198. (b) Paddon-Row, M. N. *Acc. Chem. Res.* **1994**, *27*, 18. (c) Osuka, A.; Mataga, N.; Okada, T. *Pure Appl. Chem.* **1997**, *69*, 797. (d) Verhoeven, J. W. In *Electron Transfer*; Jortner, J., Bixon, M., Eds.; John Wiley & Sons: New York, 1999; Part 1, pp 603−644. (e) Blanco, M.-J.; Jiménez, M. C.; Chambron, J.-C.; Heitz, V.; Linke, M.; Sauvage, J.-P. *Chem. Soc. Rev.* **1999**, *28*, 293.

(4) (a) Meyer, T. J. *Acc. Chem. Res.* **1989**, *22*, 163. (b) Wasielewski, M. R. *Chem. Rev.* **1992**, *92*, 435. (c) Willner, I.; Willner, B. In *Advances in Photochemistry*; Neckers, D. C., Volman, D. H., Von Bünau, G., Eds.; Wiley: London, 1995; Vol. 20, p 217. (d) Fukuzumi, S.; Guldi, D. M. In *Electron Transfer in Chemistry*; Balzani, V., Ed.; Wiley-VCH: Weinheim, 2000, in press. (e) Gust, D.; Moore, T. A. In *The Porphyrin Handbook*; Kadish, K. M., Smith, K. M., Guilard, R., Eds.; Academic Press: San Diego, CA, 2000; Vol. 8, pp 153−190.

(5) (a) *Organic and Inorganic Photochemistry*; Ramamurthy, V., Schanze, K. S., Eds.; Marcel-Dekker: New York, 1998; Vol. 2. (b) *Multimetallic and Macromolecular Inorganic Photochemistry*; Ramamurthy, V., Schanze, K. S., Eds.; Marcel-Dekker: New York, 1999; Vol. 4. (c) Balzani, V.; Juris, A.; Venturi, M.; Campagna, S.; Serroni, S. *Chem. Rev.* **1996**, *96*, 759.

(6) (a) Wagner, R. W.; Lindsey, J. S. *Pure Appl. Chem.* **1996**, *68*, 1373. (b) Li, F.; Yang, S. I.; Ciringh, Y.; Seth, J.; Martin, C. H., III; Singh, D. L.; Kim, D.; Birge, R. R.; Bocian, D. F.; Holten, D.; Lindsey, J. S. *J. Am. Chem. Soc.* **1998**, *120*, 10001. (c) Nakano, A.; Osuka, A.; Yamazaki, I.; Yamazaki, T.; Nishimura, Y. *Angew. Chem., Int. Ed.* **1998**, *37*, 3023. (d) Jiang, D.-L.; Aida, T. *J. Am. Chem. Soc.* **1998**, *120*, 10895. (e) Lammi, R. K.; Ambroise, A.; Balasubramanian, T.; Wagner, R. W.; Bocian, D. F.; Holten, D.; Lindsey, J. S. *J. Am. Chem. Soc.* **2000**, *122*, 7579. (f) Kuciauskas, D.; Liddell, P. A.; Lin, S.; Johnson, T. E.; Weghorn, S. J.; Lindsey, J. S.; Moore, A. L.; Moore, T. A.; Gust, D. *J. Am. Chem. Soc.* **1999**, *121*, 8604.

(7) (a) Imahori, H.; Sakata, Y. *Adv. Mater.* **1997**, *9*, 537. (b) Imahori, H.; Sakata, Y. *Eur. J. Org. Chem.* **1999**, 2445. (c) Guldi, D. M. *Chem. Commun.* **2000**, 321. (d) Guldi, D. M.; Prato, M. *Acc. Chem. Res.* **2000**, *33*, 695.

10.1021/ja002154k CCC: $20.00
Published on Web 12/14/2000

precluded successful development of photosynthesis-mimicking systems. On the other hand, self-assembled monolayers (SAMs) are expected to provide a highly promising way to overcome these problems.[14] There have so far been several examples of photoinduced ET[15,16] or EN[17] in SAMs on gold electrodes and semiconductors. However, artificial photosynthetic SAMs, which can exhibit both photoinduced EN and ET to yield efficient photocurrent generation, have yet to be constructed.[18]

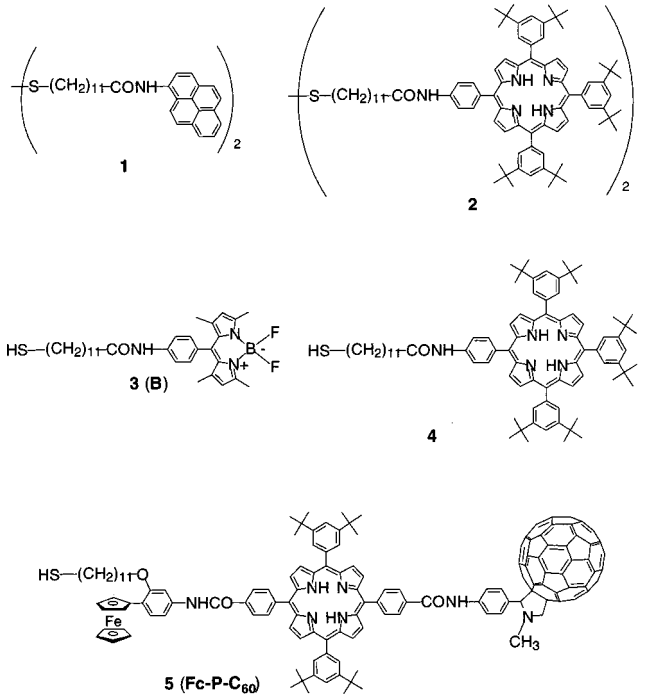

Figure 1. Structures of molecules used in this study.

Scheme 1

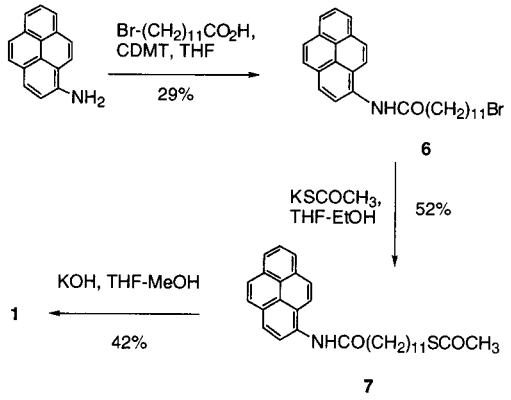

We report herein a series of the construction of integrated artificial photosynthetic assemblies on a gold electrode using mixed SAMs of energy donor and acceptor model (Figure 1). First we examined photoinduced EN in mixed SAMs of bis(pyrene) disulfide (**1**) and bis(porphyrin) disulfide (**2**) on the gold electrode in which efficient singlet−singlet EN from the pyrene to the porphyrin moiety has been detected by fluorescence lifetime measurements.[17b,19] In the next step, occurrence of photoinduced EN from the singlet excited state of the boron−dipyrrin moiety to the porphyrin moiety in mixed SAMs of boron−dipyrrin thiol (**3**) and porphyrin alkanethiol (**4**) on the gold electrode has been confirmed successfully by steady-state fluorescence spectroscopy. At the last stage of this study, we have shown the first construction of integrated artificial photosynthetic assemblies on a gold electrode using mixed SAMs of boron−dipyrrin thiol **3** as a light-harvesting molecule,

(8) (a) Seta, P.; Bienvenue, E.; Moore, A. L.; Mathis, P.; Bensasson, R. V.; Liddell, P. A.; Pessiki, P. J.; Joy, A.; Moore, T. A.; Gust, D. *Nature* **1985**, *316*, 653. (b) Steinberg-Yfrach, G.; Liddell, P. A.; Hung, S.-C.; Moore, A. L.; Gust, D.; Moore, T. A. *Nature* **1997**, *385*, 239. (c) Steinberg-Yfrach, G.; Rigaud, J.-L.; Durantini, E. N.; Moore, A. L.; Gust, D.; Moore, T. A. *Nature* **1998**, *392*, 479.

(9) (a) Fujihira, M. *Mol. Cryst. Liq. Cryst.* **1990**, *183*, 59. (b) Kim, Y.-S.; Liang, K.; Law, K.-Y.; Whitten, D. G. *J. Phys. Chem.* **1994**, *98*, 984. (c) Morita, T.; Kimura, S.; Imanishi, Y. *J. Am. Chem. Soc.* **1999**, *121*, 581. (d) Fungo, F.; Otero, L. A.; Sereno, L.; Silber, J. J.; Durantini, E. N. *J. Mater. Chem.* **2000**, *10*, 645. (e) Choudhury, B.; Weedon, A. C.; Bolton, J. R. *Langmuir* **1998**, *14*, 6199. (f) Fujihira, M.; Nishiyama, K.; Yamada, H. *Thin Solid Films* **1985**, *132*, 77.

(10) (a) Fox, M. A. *Top. Curr. Chem.* **1991**, *159*, 68. (b) Fox, M. A. *Acc. Chem. Res.* **1992**, *25*, 569. (c) Bard, A. J.; Fox, M. A. *Acc. Chem. Res.* **1995**, *28*, 141. (d) Fox, M. A. *Acc. Chem. Res.* **1999**, *32*, 201.

(11) (a) Hagfeldt, A.; Grätzel, M. *Chem. Rev.* **1995**, *95*, 49. (b) Bonhote, P.; Moser, J.-E.; Humphry-Baker, R.; Vlachopoulos, N.; Zakeeruddin, S. M.; Walder, L.; Grätzel, M. *J. Am. Chem. Soc.* **1999**, *121*, 1324. (c) Hagfeldt, A.; Grätzel, M. *Acc. Chem. Res.* **2000**, *33*, 269.

(12) (a) Mallouk, T. E.; Harrison, D. J. In *Interfacial Design and Chemical Sensing*; Mallouk, T. E., Harrison, D. J., Eds.; ACS Symposium Series 561; American Chemical Society: Washington, DC, 1994. (b) Cao, G.; Hong, H.-G.; Mallouk, T. E. *Acc. Chem. Res.* **1992**, *25*, 420. (c) Kaschak, D. M.; Lean, J. T.; Waraksa, C. C.; Saupe, G. B.; Usami, H.; Mallouk, T. E. *J. Am. Chem. Soc.* **1999**, *121*, 3435. (d) Kaschak, D. M.; Johnson, S. A.; Waraksa, C. C.; Pogue, J.; Mallouk, T. E. *Coord. Chem. Rev.* **1999**, *185*−*186*, 403.

(13) (a) *Molecular Level Artificial Photosynthetic Materials*; Meyer, G. J., Ed.; Wiley: New York, 1997. (b) Argazzi, R.; Bignozzi, C. A.; Heimer, T. A.; Castellano, F. N.; Meyer, G. J. *J. Phys. Chem. B* **1997**, *101*, 2591. (c) Kleverlaan, C. J.; Indelli, M. T.; Bignozzi, C. A.; Pavanin, L.; Scandola, F.; Hasselman, G. M.; Meyer, G. J. *J. Am. Chem. Soc.* **2000**, *122*, 2840.

(14) Ulman, A. *An Introduction to Ultrathin Organic Films*; Academic: San Diego, 1991.

(15) (a) Byrd, H.; Suponeva, E. P.; Bocarsly, A. B.; Thompson, M. E. *Nature* **1996**, *380*, 610. (b) Uosaki, K.; Kondo, T.; Zhang, X.-Q.; Yanagida, M. *J. Am. Chem. Soc.* **1997**, *119*, 8367. (c) Kondo, T.; Yanagida, M.; Nomura, S.-i.; Ito, T.; Uosaki, K. *J. Electroanal. Chem.* **1997**, *438*, 121. (d) Lahav, M.; Gabriel, T.; Shipway, A. N.; Willner, I. *J. Am. Chem. Soc.* **1999**, *121*, 258. (e) Koide, Y.; Terasaki, N.; Akiyama, T.; Yamada, S. *Thin Solid Film* **1999**, *350*, 223. (f) Morita, T.; Kimura, S.; Kobayashi, S.; Imanishi, Y. *J. Am. Chem. Soc.* **2000**, *122*, 2850. (g) Kondo, T.; Yanagida, M.; Zhang, X.-Q.; Uosaki, K. *Chem. Lett.* **2000**, 964. (h) Hatano, T.; Ikeda, A.; Akiyama, T.; Yamada, S.; Sano, M.; Kanekiyo, Y.; Shinkai, S. *J. Chem. Soc., Perkin Trans. 2*, **2000**, 909.

(16) (a) Akiyama, T.; Imahori, H.; Ajavakom, A.; Sakata, Y. *Chem. Lett.* **1996**, 907. (b) Imahori, H.; Norieda, H.; Ozawa, S.; Ushida, K.; Yamada, H.; Azuma, T.; Tamaki, K.; Sakata, Y. *Langmuir* **1998**, *14*, 5335. (c) Imahori, H.; Ozawa, S.; Ushida, K.; Takahashi, M.; Azuma, T.; Ajavakom, A.; Akiyama, T.; Hasegawa, M.; Taniguchi, S.; Okada, T.; Sakata, Y. *Bull. Chem. Soc. Jpn.* **1999**, *72*, 485. (d) Imahori, H.; Azuma, T.; Ozawa, S.; Yamada, H.; Ushida, K.; Ajavakom, A.; Norieda, H.; Sakata, Y. *Chem. Commun.* **1999**, 557. (e) Imahori, H.; Azuma, T.; Ajavakom, A.; Norieda, H.; Yamada, H.; Sakata, Y. *J. Phys. Chem. B* **1999**, *103*, 7233. (f) Imahori, H.; Yamada, H.; Ozawa, S.; Ushida, K.; Sakata, Y. *Chem. Commun.* **1999**, 1165. (g) Imahori, H.; Norieda, H.; Nishimura, Y.; Yamazaki, I.; Higuchi, K.; Kato, N.; Motohiro, T.; Yamada, H.; Tamaki, K.; Arimura, M.; Sakata, Y. *J. Phys. Chem. B* **2000**, *104*, 1253. (h) Imahori, H.; Yamada, H.; Nishimura, Y.; Yamazaki, I.; Sakata, Y. *J. Phys. Chem. B* **2000**, *104*, 2099. (i) Hirayama, D.; Yamashiro, T.; Takimiya, K.; Aso, Y.; Otsubo, T.; Norieda, H.; Imahori, H.; Sakata, Y. *Chem. Lett.* **2000**, 570. (j) Yamada, H.; Imahori, H.; Nishimura, Y.; Yamazaki, I.; Fukuzumi, S. *Chem. Commun.* **2000**, 1921. (k) Fukuzumi, S.; Imahori, H. In *Electron Transfer in Chemistry*; Balzani, V., Ed.; Wiley-VCH: Weinheim, 2000, in press.

(17) (a) Meyer, T. J.; Meyer, G. J.; Pfennig, B. W.; Schoonover, J. R.; Timpson, C. J.; Wall, J. F.; Kobusch, C.; Chen, X.; Peek, B. M.; Wall, C. G.; Ou, W.; Erickson, B. W.; Bignozzi, C. A. *Inorg. Chem.* **1994**, *33*, 3952. (b) Imahori, H.; Nishimura, Y.; Norieda, H.; Karita, H.; Yamazaki, I.; Sakata, Y.; Fukuzumi, S. *Chem. Commun.* **2000**, 661. (c) Chrisstoffels, L. A. J.; Adronov, A.; Fréchet, J. M. J. *Angew. Chem., Int. Ed.* **2000**, *39*, 2163.

(18) Although SAMs integrating photoenergy-harvesting and electron-transport systems have recently been reported, there is no significant integrating effect because of the poor photocurrent generation (∼100 pA) and quantum yield (∼0.3−0.4%); see: Morita, T.; Kimura, S.; Kobayashi, S.; Imanishi, Y. *Chem. Lett.* **2000**, 676.

(19) Pyrene SAMs on gold surfaces have been reported by other groups; see: (a) Karpovich, D. S.; Blanchard, G. J. *Langmuir* **1996**, *12*, 5522. (b) Fox, M. A.; Whitesell, J. K.; McKerrow, A. J. *Langmuir* **1998**, *14*, 816.

Scheme 2

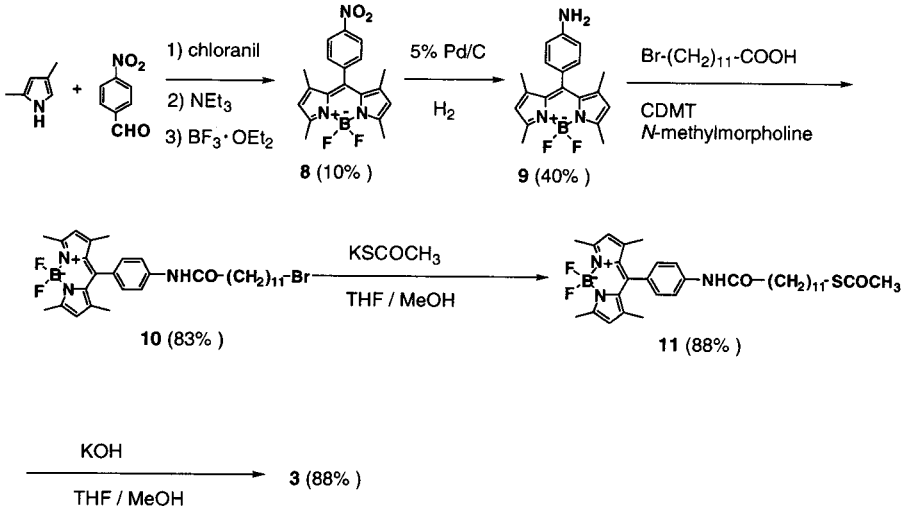

combined with a reaction center model, ferrocene−porphyrin−fullerene triad thiol (**5**). The highest quantum efficiency (50 ± 8%, based on the adsorbed photons) ever reported for generation of the photocurrent output has been accomplished by a cascade of photoinduced EN and multistep ET in mixed SAMs of **3** and **5**.

Results and Discussion

Synthesis. The synthetic routes to **1** and **3** are shown in Scheme 1 and Scheme 2, respectively. Condensation of 1-aminopyrene with 12-bromododecanoic acid in the presence of 2-chloro-4,6-dimethoxy-1,3,5-triazine (CDMT) afforded **6** in 29% yield. Bromide **6** was converted to bis(pyrene) disulfide **1** via nucleophilic substitution with potassium thioacetate and subsequent base deprotection of **7** (Scheme 1).[20]

Boron−dipyrrin thiol **3** was synthesized by following the similar procedure (Scheme 2). 2,4-Dimethylpyrrole was condensed with 4-nitrobenzaldehyde to form dipyrromethane, which was oxidized and treated with BF_3·Et_2O to yield **8** in 10% yield.[21] Reduction of nitro group of **8** afforded amino boron−dipyrrin dye **9** in 40% yield.[16e] Condensation of **9** with 12-bromododecanoic acid in the presence of CDMT gave **10** in 83% yield.[20] Bromide **10** was converted to thiol **3** via nucleophilic substitution with potassium thioacetate and subsequent base deprotection of **11** (Scheme 2).[20]

Bis(porphyrin) disulfide **2**[16g] and ferrocene−porphyrin−C_{60} alkanethiol **5**[16h] were prepared by following the same procedures as described previously. Porphyrin thiol **4** was obtained by modifying the original procedures slightly.[16g] Their structures were verified by spectroscopic analyses (see Experimental Section).

Mixed SAMs of Pyrene and Porphyrin. At first mixed SAMs of pyrene and porphyrin were prepared to examine the possibility of photoinduced EN in SAMs. Monolayers of mixtures of **1** and **2** were formed by the coadsorption of **1** and **2** onto Au(111)mica substrates (hereafter denoted as **1**,**2**/Au, where / represents an interface). The coadsorption onto the gold surface was carried out from CH_2Cl_2 solutions containing **1** and **2** with the total concentration of 10 μM (molar ratio of **1**:**2** = (a) 100:0, (b) 90:10, (c) 50:50, (d) 10:90, (e) 0:100) for 20 h to complete the mixed SAM formation. After soaking, the gold substrate was washed well with CH_2Cl_2 and dried with a stream of argon.

The cyclic voltammetric measurements of **1**,**2**/Au in CH_2Cl_2 containing 0.1 M *n*-Bu_4NPF_6 electrolyte were performed with a sweep rate of 50 mV s^{-1} (electrode area, 0.48 cm^2) to estimate the surface coverage (Figure 2). Two successive redox couples, corresponding to the first and second oxidation of the porphyrin moiety (E^0_{ox} = +1.10, +1.33 V vs Ag/AgCl (saturated KCl)), are clearly seen for **2**/Au in Figure 2a,[16g] whereas a broad redox wave, due to the first oxidation of the pyrene moiety (E^0_{ox} = +0.95 V vs Ag/AgCl), was observed for **1**/Au in Figure 2b. The adsorbed amounts of **1** and **2** on **1**/Au (**1**:**2** = (a) 100:0) and **2**/Au (**1**:**2** = (e) 0:100) were calculated from the anodic peak currents of the pyrene and the porphyrin moieties as 2.8 × 10^{-10} mol cm^{-2} (=59 $Å^2$ $molecule^{-1}$)[22] and 1.5 × 10^{-10} mol cm^{-2} (=110 $Å^2$ $molecule^{-1}$),[16g] respectively. These values indicate the formation of well-packed structures of **1** and **2** on the gold surface. In the mixed SAMs, however, the waves due to the first oxidation of the pyrene and porphyrin moieties in Figure 2c are too broad to determine accurately the adsorbed amounts of **1** and **2** in **1**,**2**/Au (**1**:**2** = (c) 50:50).

The absorption spectra of **1** and **2** in CH_2Cl_2 and of **1**,**2**/Au (**1**:**2** = (c) 50:50) measured using transmission mode in air are shown in Figure 3 (part a−c, respectively). The absorption bands of **1** (λ_{max} = 337 nm) and **2** (λ_{max} = 424 nm) in the mixed SAM (**1**,**2**/(50:50)) on the gold surface (Figure 3c) are slightly blue- and red-shifted by 7 and 3 nm, as compared to those of **1** (Figure 3a) and **2** (Figure 3b)[16g] in CH_2Cl_2, respectively. Assuming that the molar absorption coefficients of **1** and **2** in the mixed SAMs are the same as those of **1**/Au and **2**/Au (**1**: 2.5 × 10^7 mol^{-1} cm^2 (λ_{max} = 337 nm); **2**: 2.3 × 10^8 mol^{-1} cm^2 (λ_{max} = 428 nm)), the relative ratios of **1**:**2** in the mixed SAMs prepared from CH_2Cl_2 solutions containing different ratios of **1**:**2** are estimated as (a) 100:0, (b) 97:3, (c) 86:14, (d) 72:28, and (e) 0:100 (Table 1). The estimated ratios of **1**:**2** in the **1**,**2**/Au, (b)−(d), are significantly higher than those of the solution: (b) 90:10, (c) 50:50, (d) 10:90. The strong $\pi-\pi$

(20) (a) Wolf, M. O.; Fox, M. A. *J. Am. Chem. Soc.* **1995**, *117*, 1845. (b) Wolf, M. O.; Fox, M. A. *Langmuir* **1996**, *12*, 955. (c) Fox, M. A.; Wooten, M. D. *Langmuir* **1997**, *13*, 7099. (d) Li, W.; Lynch, V.; Thompson, H.; Fox, M. A. *J. Am. Chem. Soc.* **1997**, *119*, 7211. (e) Reese, S.; Fox, M. A. *J. Phys. Chem. B* **1998**, *102*, 9820.

(21) Debreczeny, M. P.; Svec, W. A.; Wasielewski, M. R. *New J. Chem.* **1996**, *20*, 815.

(22) Densely packed monolayer films are known to retard ion transport and electrochemical accessibility. Since pyrene is a planar aromatic molecule, the pyrene moiety of **1** may be densely packed due to the strong $\pi-\pi$ stacking in the monolayers. Thus, the actual value of surface coverage may be larger, as compared to the estimated value (2.8 × 10^{-10} mol cm^{-2}) using cyclic voltammetry; see: Campbell, D. J.; Herr, B. R.; Hulteen, J. C.; Van Duyne, R. P.; Mirkin, C. A. *J. Am. Chem. Soc.* **1996**, *118*, 10211.

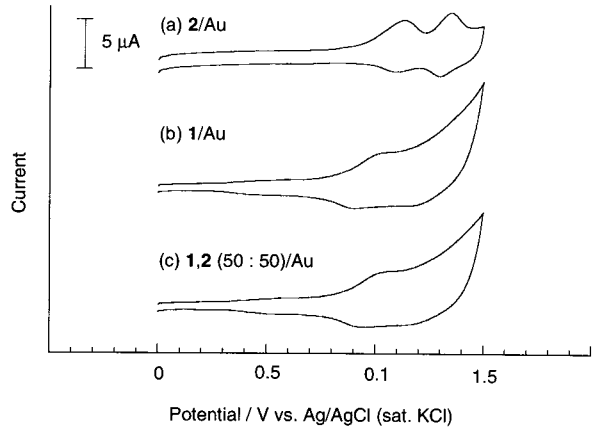

Figure 2. Cyclic voltammograms of (a) a SAM of **2** (**2**/Au, top), (b) a SAM of **1** (**1**/Au, middle), and (c) a mixed SAM of **1** and **2** on the gold surface (**1**,**2** (50:50)/Au, bottom) from the CH_2Cl_2 solution with a molar ratio of 50:50. The cyclic voltammograms of **1**,**2**/Au in CH_2Cl_2 containing 0.1 M *n*-Bu_4NPF_6 electrolyte were obtained with a sweep rate of 50 mV s^{-1} (electrode area, 0.48 cm^2).

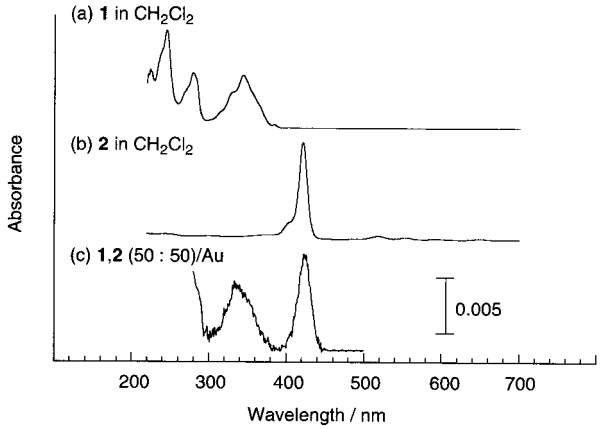

Figure 3. Absorption spectra of (a) **1** in CH_2Cl_2 and (b) **2** in CH_2Cl_2 and (c) mixed SAM of **1** and **2** on the gold surface (**1**,**2** (50:50)/Au) from the CH_2Cl_2 solution with a molar ratio of 50:50. The spectra of **1** and **2** in CH_2Cl_2 are normalized for comparison.

Table 1. Concentration Dependence of Surface Coverage and Fluorescence Lifetime in Au/**1**,**2**

1:**2**[a] solution	**1**:**2**[b] mixed SAMs	surface coverage/10^{-10} mol cm^{-2},[b] (absorbance)[c] **1**	**2**	fluorescence lifetimes (τ)/ns[d] λ_{obs} = 385 nm	λ_{obs} = 720 nm
100:0	100:0	2.8 (0.0070)	0	0.023	
90:10	97:3	2.7 (0.0068)	0.093 (0.0021)	0.020	0.092
50:50	86:14	2.4 (0.0059)	0.39 (0.0089)	0.011	0.088
10:90	72:28	2.2 (0.0056)	0.84 (0.019)	0.0088	0.060
0:100	0:100	0	1.5 (0.034)		0.040

[a] Molar ratio of **1**:**2** in CH_2Cl_2 solutions with the total concentration of 10 μM for formation of the mixed SAMs. [b] Molar ratio of **1**:**2** on the gold electrodes estimated from the electrochemical and absorption measurements. [c] Absorbance at the λ_{max} (**1**: 337 nm; **2**: ~428 nm) on the gold surface. [d] Excitation at 280 nm.

interaction of the pyrene moieties as compared to the relatively weak interaction between the porphyrin moieties due to the bulky *tert*-butyl groups may be responsible for the preference of the adsorption of **1** over **2** on the gold surface. In addition, the fact that the pyrene molecules occupy about half the surface area of the porphyrins would lead to a thermodynamic preference for pyrene adsorption, since displacement of a porphyrin for two pyrenes results in an extra S−Au interaction.

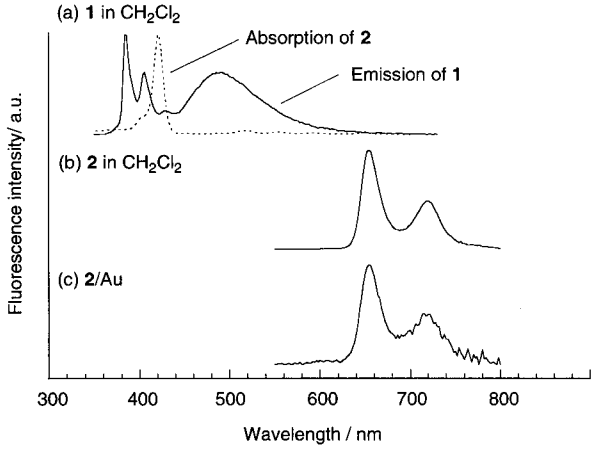

Figure 4. Fluorescence spectra of (a) **1** (absorption spectra of **2** in CH_2Cl_2 is shown as dotted line) and (b) **2** in CH_2Cl_2 and (c) SAM of **2** on the gold surface (**2**/Au, λex = 428 nm) with excitation at 344 nm for **1** and 421 nm for **2**. The spectra are normalized for comparison.

Steady-state fluorescence spectra of **1** and **2** in CH_2Cl_2 were measured with the excitation wavelength at the respective absorption maximum, 344 and 421 nm. The fluorescence emission of **1** in Figure 4a (solid line) overlaps well with absorption of **2** in Figure 4a (dotted line). The fluorescence spectrum of **2**/Au (Figure 4c) is essentially the same as that of **2** in CH_2Cl_2 (Figure 4b).[16g] Thus, it is expected that excitation of the pyrene moiety in **1** as an antenna chromophore may lead to an efficient singlet−singlet EN from the pyrene (3.33 eV) to the porphyrin (1.90 eV) moiety in the SAMs. Unfortunately, however, the emission of **1**/Au was too weak to be detected. No detectable fluorescence from the pyrene or the porphyrin moiety was observed in **1**,**2**/Au under the steady-state irradiation.

To probe a singlet−singlet EN from the pyrene to the porphyrin moiety in the SAMs, time-resolved, single-photon counting fluorescence measurements were performed for **1**,**2**/Au (**1**:**2** = (a) 100:0, (b) 90:10, (c) 50:50, (d) 10:90, (e) 0:100) as well as **1** and **2** in solutions with the excitation wavelength at 280 nm, where the light is mainly absorbed by the pyrene moiety (Figure 3). In each case the decay of the fluorescence intensity at λ_{obs} = 385 nm and λ_{obs} = 720 nm (due to the singlet excited states of the pyrene and the porphyrin, respectively) could be monitored (Figure 4). The decay curve could be fitted as single exponential except for the case of **1** at 385 nm in CH_2Cl_2. The fluorescence lifetimes of **1**/Au at 385 nm (23 ps) and **2**/Au at 720 nm (40 ps) were much shorter than those of **1** (7.4 ns (30%), 3.2 ns (70%)) and **2** (8.1 ns) in CH_2Cl_2. This indicates that the excited singlet states of the pyrene and the porphyrin moieties in the SAMs are efficiently quenched by an EN to the gold surface.[16g] However, it is important to note that the fluorescence lifetimes of the pyrene moiety in **1**,**2**/Au at 385 nm decrease with an increase in the relative ratio of the porphyrin to the pyrene ((a) 23 ps, (b) 20 ps, (c) 11 ps, (d) 8.8 ps) (Table 1).[23] The fluorescence lifetimes of the porphyrin moiety in **1**,**2**/Au at 720 nm also decrease with an increase in the relative ratio of the porphyrin to the pyrene ((b) 92 ps, (c) 88 ps,(d) 60 ps, (e) 40 ps). Thus, efficient EN (>62%) may occur from the excited singlet state of the pyrene to the porphyrin, followed by energy migration among the porphyrins.[24]

(23) Both monomer emission (~400 nm) and excimer emission (~500 nm) were observed for **1** in CH_2Cl_2, as shown in Figure 4a. The fluorescence lifetimes of **1**,**2**/Au at 500 nm also decreased with an increase in the relative ratio of the porphyrin to the pyrene.

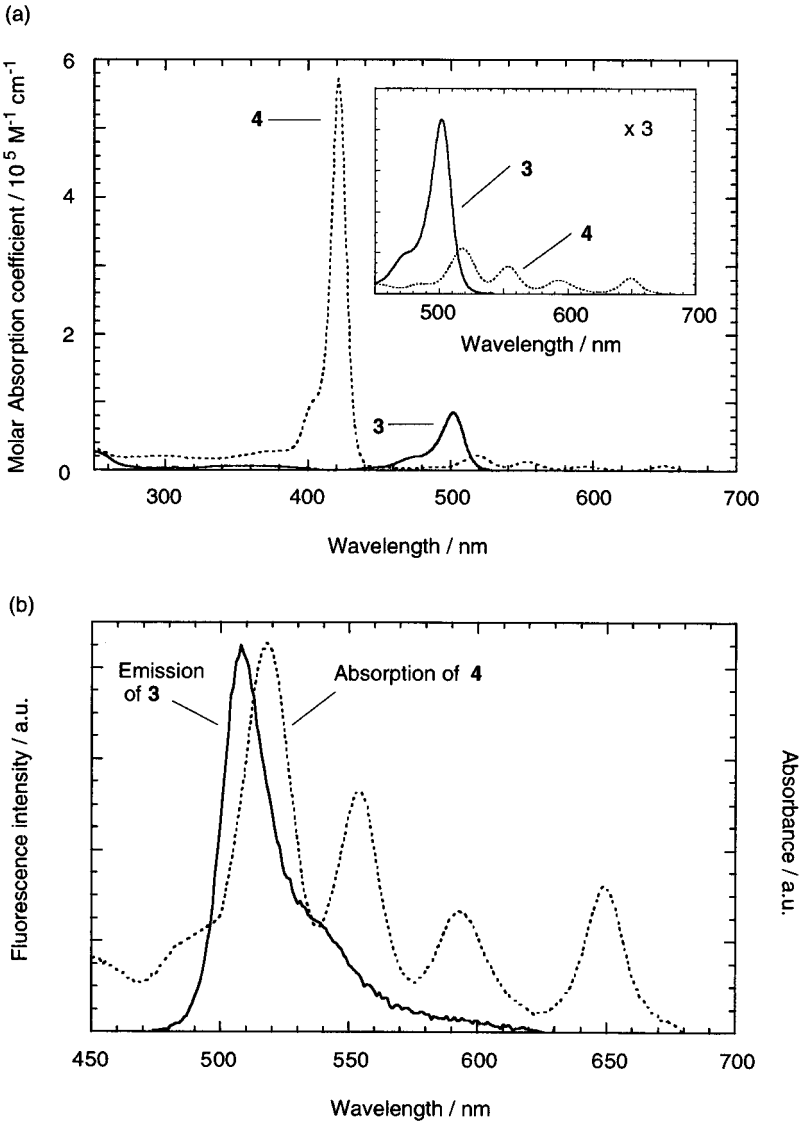

Figure 5. (a) Absorption spectra of **3** (solid line) and **4** (dotted line) in CH_2Cl_2. Inset depicts the expanded spectra (×3) at 450−700 nm. (b) Fluorescence spectrum of **3** in CH_2Cl_2 (solid line) with excitation at 450 nm. The absorption spectrum of **4** in CH_2Cl_2 (dotted line) is normalized at the peak position for comparison.

Mixed SAMs of Boron−Dipyrrin Dye and Porphyrin. Although an efficient singlet−singlet EN takes place from the pyrene to the porphyrin moiety in the mixed SAMs of pyrene and porphyrin on the gold surface (vide supra), pyrene can absorb light only in the ultraviolet region (λ_{max} = 337 nm), thereby making it impossible to harvest light in the visible region. Boron−dipyrrin thiol (**3**) was then chosen as the much better light-harvesting molecule[6a,b] to achieve an efficient EN from the boron−dipyrrin moiety (^{1}B*) in **3** to the porphyrin moiety (P) of an energy acceptor model (porphyrin alkanethiol **4**). The boron−dipyrrin dye (B in **3**) exhibits a moderately strong absorption band in the visible region at 502 nm ($\epsilon = 8.5 \times 10^4$ M^{-1} cm^{-1}) and a relatively long singlet excited-state lifetime (~5 ns).[25] Since the porphyrin moiety in **4**, a major absorber of photons, absorbs strongly in the blue (~420 nm) and weakly in the green region, an incorporation of the boron−dipyrrin pigments **3** into a SAM of **4** (denoted as **4**/Au) makes it possible to enhance the absorption properties in the green region as well as the blue region as shown in Figure 5a. More importantly, the emission from the boron−dipyrrin overlaps well with the absorption of the porphyrin in solutions (Figure 5b). Thus, a singlet−singlet efficient EN from the boron−dipyrrin moiety (^{1}B*) in **3** to the porphyrin moiety (P) in **4** is expected to occur in the mixed SAMs of **3** and **4** on the gold surface (denoted as **3**,**4**/Au).

The singlet excitation energy of **3** on the gold surface was estimated as 2.43 eV from the absorption and fluorescence spectra of **3** on the gold surface (denoted as **3**/Au). The one-electron oxidation potential (E^0_{ox}) of **3**/Au was determined as 1.25 V (vs Ag/AgCl) from the cyclic voltammogram (Figure 6a).[26] From these values, the one-electron redox potential of ^{1}B*/B$^{\bullet+}$ is determined as −1.18 V. The energy levels of other components of our artificial photosynthetic SAM system are already known,[16g,h] and they are summarized in Scheme 3.

(24) Hirakawa, K.; Segawa, H. *J. Photochem. Photobiol. A* **1999**, *123*, 67.

(25) Karolin, J.; Johansson, L. B.-A.; Strandberg, L.; Ny, T. *J. Am. Chem. Soc.* **1994**, *116*, 7801.

(26) The cyclic voltammogram of **3**/Au is characterized by a anodic wave showing a well-defined current maximum but much smaller coupled cathodic wave on the reversed scan at 100 mV s^{-1} due to the instability of the radical cation. The cathodic current maximum increases with an increase in the scan rate. The E^0_{ox} value was determined as the average of the anodic and cathodic peak potentials.

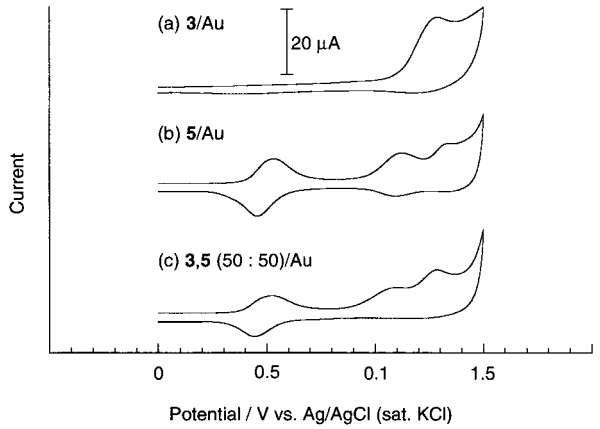

Figure 6. Cyclic voltammograms of (a) a SAM of **3** (**3**/Au), (b) a SAM of **5** (**5**/Au), and (c) a mixed SAM of **3** and **5** on the gold surface (**3**,**5** (50:50)/Au) from the CH_2Cl_2 solution with a molar ratio of 50:50. The cyclic voltammograms of **3**,**5**/Au in CH_2Cl_2 containing 0.1 M *n*-Bu_4NPF_6 electrolyte were obtained with a sweep rate of 100 mV s^{-1} (electrode area, 0.48 cm^2).

Scheme 3

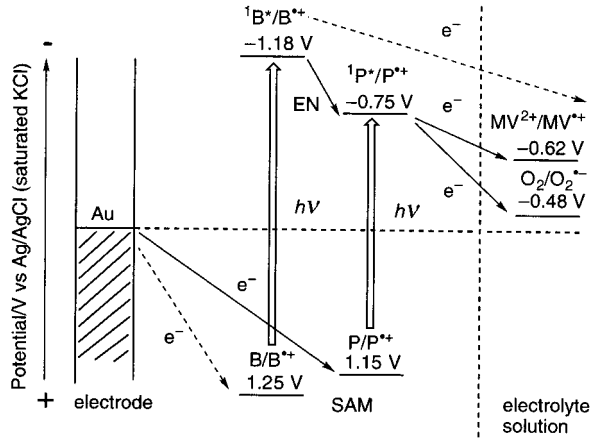

On the basis of the energy diagram in Scheme 3, an EN is expected to take place from ^{1}B* in **3** to P in **4**, followed by an intermolecular ET from the resulting porphyrin singlet excited state (^{1}P*) to a diffusing electron carrier such as O_2 ($O_2/O_2^{\bullet -} = -0.48$ V)[16g,h,27] and methyl viologen (MV^{2+}) ($MV^{2+}/MV^{\bullet +} = -0.62$ V),[16g,h,27] which eventually gives an electron to the counter electrode. On the other hand, the gold electrode gives an electron to the porphyrin radical cation ($P^{\bullet +}$), generating vectorial electron flow from the gold electrode to the counter electrode through the SAM and the electrolyte. Thus, the present SAM system is expected to mimic both photosynthetic EN and ET in the mixed SAMs.

The mixed SAMs of **3** and **4** (denoted as **3**,**4**/Au) were prepared by the coadsorption from a CH_2Cl_2 solution containing **3** and **4** with the total concentration of 10 μM (molar ratio of **3**:**4** = (a) 100:0, (b) 90:10, (c) 75:25, (d) 50:50, (e) 25:75, (f) 0:100). Cyclic voltammogram measurements were performed using **3**,**4**/Au in CH_2Cl_2 containing 0.1 M *n*-Bu_4NPF_6 electrolyte with a sweep rate of 100 mV s^{-1} (electrode area, 0.48 cm^2) to estimate the surface coverage. The electrochemical behavior of **4**/Au was similar to that of **2**/Au (Figure 2a). Adsorbed amounts of **3** and **4** on **3**/Au (**3**:**4** = (a) 100:0) and **4**/Au (**3**:**4** = (f) 0:100) were estimated from the charge of the anodic peak of the boron−dipyrrin and the porphyrin moieties as 3.7×10^{-10} mol cm^{-2} (= 45 $Å^2$ $molecule^{-1}$) and 1.5×10^{-10} mol cm^{-2} (= 110 $Å^2$ $molecule^{-1}$), respectively. These values suggest the formation of well-packed structures of **3** and **4** on the gold surface. In the mixed SAMs, however, the overlapped waves due to the first oxidation of the boron−dipyrrin and porphyrin moieties were too broad to determine accurately the adsorbed amounts of **3** and **4** in **3**,**4**/Au (**3**:**4** = (d) 50:50), as in the case of **1** and **2** in **1**,**2**/Au (Figure 2c).

The adsorbed amounts of **3** and **4** in **3**,**4**/Au were then estimated from the absorption spectra of mixed SAMs of **3** and **4** on the gold surface, assuming that the molar absorption coefficients of **3** and **4** in the mixed SAMs are the same as those of **3**/Au and **4**/Au [**3**: 4.1×10^7 mol^{-1} cm^2 (λ_{max} = 510 nm); **4**: 2.3×10^8 mol^{-1} cm^2 (λ_{max} = 428 nm)] (Table 2). The estimated relative ratios of **3**:**4** in the mixed SAMs (the values in solution are given in parentheses) are (b) 95:5 (90:10), (c) 90:10 (75:25), (d) 84:16 (50:50), and (e) 69:31 (25:75) which are significantly higher than those of the solution as in the case of the ratios of **1**:**2** in **1**,**2**/Au (Tables 1 and 2). The preference of the adsorption of **3** over **4** on the gold surface may also result from the strong $\pi-\pi$ interaction of the boron−dipyrrin moieties against relatively weak interaction between the porphyrin moieties due to the bulky *tert*-butyl groups and the thermodynamic preference for boron−dipyrrin adsorption against the porphyrin which has the larger occupied area (vide supra).

An efficient EN from **3** to the porphyrin moiety in **4** was confirmed by the fluorescence spectrum of **3**,**4**/Au which revealed emission only from the porphyrin moiety (λ_{max} = 650, 720 nm) irrespective of excitation wavelength of either **3** (λ_{ex} = 510 nm) or **4** (λ_{ex} = 420 nm) as shown in Figure 7a. The excitation spectrum of **3**,**4**/Au with the fixed emission wavelength (λ_{em} = 650 nm) matches well with the absorption spectrum of **3**,**4**/Au as shown in Figure 7b. The EN efficiency was determined by a comparison between the excitation and absorption spectra of the mixed SAMs on the gold surface. The EN efficiency from ^{1}B* in **3** to P in **4** increases with increasing the relative ratio of the porphyrin to the boron−dipyrrin, to reach the maximum value of ∼100% at the **3**:**4** ratio of 69:31 (Table 2). This clearly indicates that an efficient EN takes place from ^{1}B* in **3** to P in **4** in the mixed SAMs of **3** and **4** on the gold surface.[28]

The photoelectrochemical measurements were performed using the SAM of **3** and **4** on the gold electrodes in a three electrode system, denoted as Au/**3**,**4**/MV^{2+}/Pt cell, under the optimized conditions previously [electrolyte solution: O_2-saturated 0.1 M Na_2SO_4 solution containing 30 mM methyl viologen dichloride (MV^{2+}) as an electron carrier; input power: 380 μW cm^{-2}; applied potential: −200 mV vs Ag/AgCl].[16g,h,27] A stable cathodic photocurrent from the gold electrode to the platinum counter electrode through the SAM appeared immediately upon irradiation of the gold electrode and the photocurrent fell down instantly when the irradiation was turned off as shown in Figure 8. An increase in the cathodic photocurrent with increasing the negative bias to the gold electrode demonstrates that the photocurrent flows from the gold electrode to the counter electrode through the SAM and the

(27) It is well-known that O_2 acts as an electron acceptor in the similar photoelectrochemical cells.[9b] O_2 bubbling of the electrolyte solution in Au/**2**/Pt cell increased the photocurrent by ∼20−30% and successive Ar bubbling of the solution decreased it nearly to the initial state both in the absence and the presence of MV^{2+}.[16g] The results indicate that O_2 is an efficient electron carrier in the Au/**2**/Pt cell. Addition of MV^{2+} (up to 5 mM) in the Au/**2**/Pt cell increased the photocurrent by about 15%, showing that MV^{2+} is also an electron carrier.[16g] However, further addition of MV^{2+} did not change the intensity of the photocurrent significantly.[16g]

(28) In the fluorescence lifetime measurements, however, the laser excitation at 261 nm of the boron−dipyrrin in **3**,**4**/Au (or **3**,**5**/Au) gave no detectable fluorescence due to the weak absorbance at the excitation wavelength (Figure 5a).

Table 2. Concentration Dependence of Surface Coverage, Energy Transfer Efficiency, and Quantum Yield in Au/**3**,**4**

		surface coverage/10^{-10} mol cm$^{-2,b}$ (absorbance)^c			quantum yield ϕ/%^{e}	
3:**4**^{a} solution	**3**:**4**^{b} mixed SAMs	**3**	**4**	EN efficiency /%^{d}	510 nm	430 nm
100:0	100:0	3.7 (0.015)	0	0	1.6 ± 0.3	
90:10	95:5	3.4 (0.014)	0.17 (0.0040)	55		
75:25	90:10	3.4 (0.014)	0.37 (0.0085)	85		
50:50	84:16	3.2 (0.013)	0.61 (0.014)	90	1.6 ± 0.3	1.9 ± 0.3
25:75	69:31	2.1 (0.0087)	0.96 (0.022)	~100		
0:100	0:100	0	1.5 (0.034)			1.8 ± 0.3

^{a} Molar ratio of **3**:**4** in CH_2Cl_2 solutions with the total concentration of 10 μM for formation of the mixed SAMs. ^{b} Molar ratio of **3**:**4** on the gold electrodes estimated from the electrochemical and absorption measurements. ^{c} Absorbance at the λ_{max} (**3**: 510 nm; **4**: ~428 nm) on the gold surface. ^{d} Estimated from excitation and absorption spectra on the gold surface. ^{e} $\phi = (i/e)/[I(1 - 10^{-A})]$, $I = (W\lambda)/(hc)$ where i is the photocurrent density, e is the elementary charge, I is number of photons per unit area and unit time, λ is the wavelength of light irradiation, A is absorbance of the adsorbed dyes at λ nm, W is light power irradiated at λ nm, c is the light velocity, and h is Planck's constant.

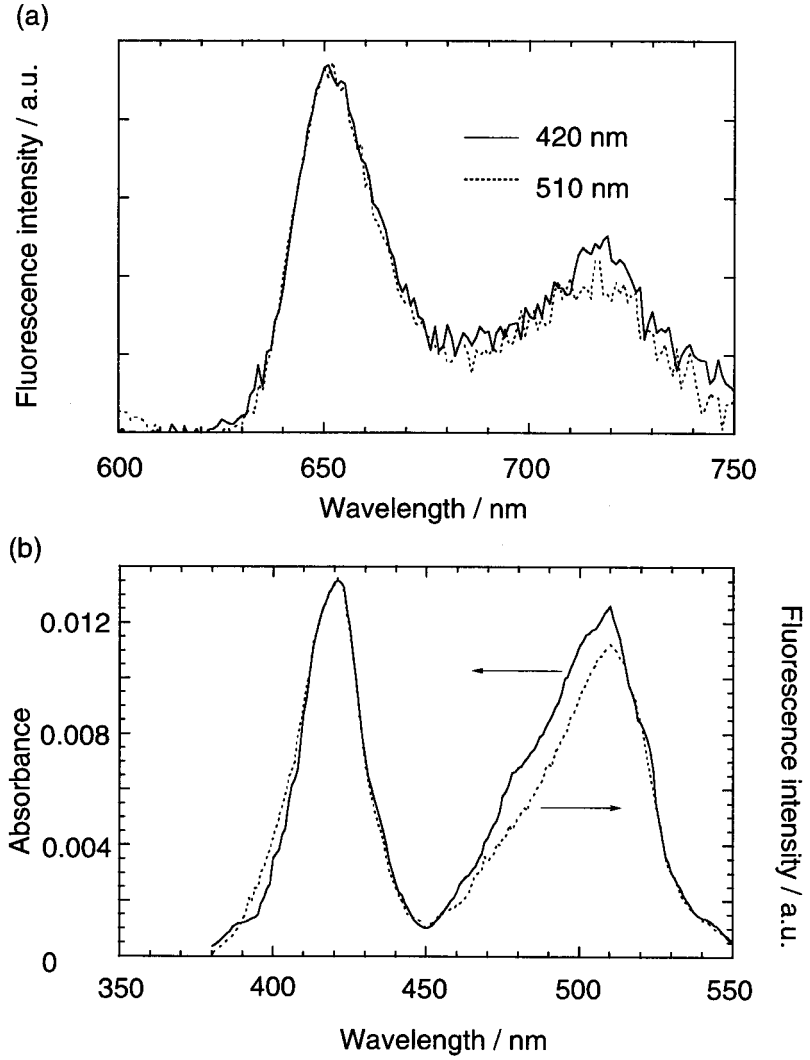

Figure 7. (a) Fluorescence spectra of a mixed SAM of **3** and **4** on the gold surface (**3**,**4** (50:50)/Au) from the CH_2Cl_2 solution with a molar ratio of 50:50 with excitation at 420 nm (solid line) and 510 nm (dotted line). (b) Absorption spectrum (solid line) and excitation spectrum (dotted line, λ_{em} = 650 nm) of **3**,**4** (50:50)/Au. The excitation spectrum is normalized at the Soret band for comparison.

electrolyte. The applied potential (−200 mV) was chosen to maximize the photocurrent, whereas the dark current is negligible.[16g,h]

The action spectra of Au/**3**/MV^{2+}/Pt cell, Au/**4**/MV^{2+}/Pt cell, and Au/**3**,**4** (50:50)/MV^{2+}/Pt cell are shown in Figure 9. The agreement of the action spectrum of Au/**3**,**4** (50:50)/MV^{2+}/Pt cell with the absorption spectrum of Au/**3**,**4** (50:50) in Figure 7b demonstrates clearly that the porphyrin and the boron−dipyrrin moieties are the photoactive species. Similar agreement between the action spectrum and absorption spectrum was obtained for Au/**3**/MV^{2+}/Pt and Au/**4**/MV^{2+}/Pt cells. Thus, photoinduced ET occurs from $^1B^*$ in **3** (or porphyrin excited singlet state ($^1P^*$) in **4**) to the electron carriers (O_2 and MV^{2+}),[27] followed by charge-shift from the gold electrode to $B^{\bullet+}$ in **3** (or $P^{\bullet+}$ in **4**), producing the cathodic current (Scheme 3). Unfortunately, however, the quantum yield (based on the absorbed photons) of Au/**3**/MV^{2+}/Pt cell (1.6 ± 0.3% at 510 nm), Au/**4**/MV^{2+}/Pt cell (1.8 ± 0.3% at 430 nm), and Au/**3**,**4**

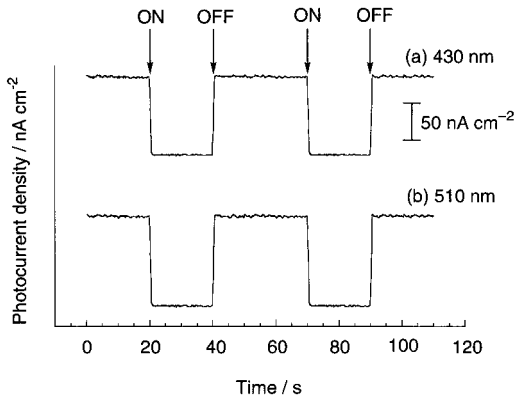

Figure 8. Photoelectrochemical response of Au/**3**,**4** (50:50)/MV^{2+}/Pt cell with illumination (a) at 430 nm and (b) 510 nm; electrolyte solution: O_2-saturated 0.1 M Na_2SO_4 solution containing 30 mM methyl viologen (MV^{2+}) as an electron carrier; input power: 380 μW cm^{-2}; applied potential: −200 mV vs Ag/AgCl (saturated KCl).

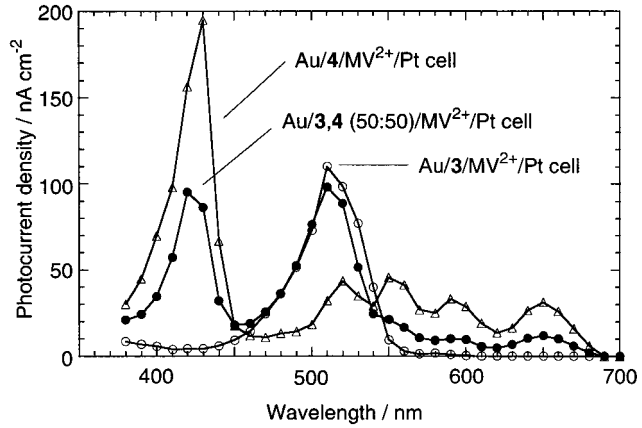

Figure 9. Action spectra of Au/**3**,**4** (50:50)/MV^{2+}/Pt cell (solid line with solid circles), Au/**3**/MV^{2+}/Pt cell (solid line with open circles), and Au/**4**/MV^{2+}/Pt cell (solid line with triangles); electrolyte solution: O_2-saturated 0.1 M Na_2SO_4 solution containing 30 mM methyl viologen (MV^{2+}) as an electron carrier; input power: 380 μW cm^{-2}; applied potential: −200 mV vs Ag/AgCl (saturated KCl).

(50:50)/MV^{2+}/Pt cell (1.6 ± 0.3% at 510 nm and 1.9 ± 0.3% at 430 nm) are similar under the same conditions. Accordingly, we could not obtain clear evidence for the photocurrent generation resulting from photoinduced EN between ^{1}B* in **3** and the porphyrin in **4** in the mixed SAMs of **3** and **4** on the gold electrode.

Mixed SAMs of Boron−Dipyrrin Dye and Ferrocene−Porphyrin−Fullerene Triad. At the last stage of this study, ferrocene (Fc)-porphyrin (P)-C_{60} triad (**5** in Figure 1) is incorporated into the boron−dipyrrin SAM system to improve the quantum yield for the photocurrent generation. The triad thiol **5** has been designed to achieve two-step ET within a molecule itself in SAMs of **5**: photoinduced ET from the porphyrin to the C_{60}, followed by the efficient charge-shift from the ferrocene to the resulting porphyrin radical cation, to yield the final charge separated state, $Fc^+-P-C_{60}^{\bullet-}$. The $C_{60}^{\bullet-}$ moiety in the charge-separated state gives an electron to an electron carrier such as MV^{2+} and O_2, whereas an electron is donated from the gold electrode to the Fc^+ moiety, resulting in the cathodic photocurrent generation as shown in Scheme 4.[16h] The energy levels of the ferrocene and C_{60} moieties in Scheme 4 have been determined from the electrochemical measurements[16h] and those of the other components are the same as given in Scheme 3.

Scheme 4

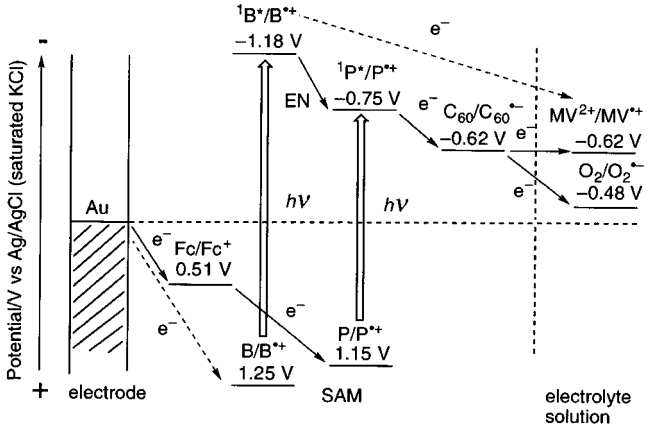

Since C_{60} has an extremely small reorganization energy of ET, forward ET is accelerated whereas back ET is retarded in multistep ET processes.[7,29] This is consistent with efficient formation of $Fc^+-P-C_{60}^{\bullet-}$ state, which has been confirmed by transient absorption measurements in solutions.[16h,30] In this context, the photocurrent generation efficiencies (quantum yield) in the triad cell are reported to be 20−25%,[16h] which are the highest values ever reported for photocurrent generation at monolayer-modified metal electrodes, as well as across artificial membranes using donor−acceptor linked molecules.[7−9,14−18] Furthermore, absorption of the porphyrin moiety in **5**, a major absorber of photons, is similar to that of **4** (Figure 5), except for the broad weak absorption due to the C_{60} in the ultraviolet region (300−400 nm) as shown in Figure 10. Accordingly, an incorporation of the boron−dipyrrin pigments **3** into **5**/Au also allows us to enhance the absorption properties in the green-region as well as the blue region. In addition, the emission from the boron−dipyrrin in **3** overlaps well with the absorption of the porphyrin in **5** (see inset of Figure 10), as seen in the case of mixed SAMs of **3** and **4** (Figure 5b). Thus, an efficient EN from the boron−dipyrrin moiety (^{1}B*) in **3** to the porphyrin moiety (P) in **5** can take place in the mixed SAMs of **3** and **5** on the gold surface (Scheme 4). Overall, it is expected that boron−dipyrrin SAM combined with ferrocene−porphyrin−C_{60} triad SAM can lead to efficient photocurrent generation, in addition to a mimicry of coupled photoinduced EN and multistep ET in photosynthesis.

The amounts of **3** and **5** on the gold surface were systematically changed by the competitive coadsorption onto the gold surface from CH_2Cl_2 solutions containing various molar ratios of **3** and **5** with the total concentration of 10 μM (molar ratio of **3**:**5** = (a) 100:0, (b) 90:10, (c) 75:25, (d) 50:50, (e) 25:75, (f) 0:100). From the cyclic voltammetric and absorption spectral data, the surface coverage of **3** and **5**, and the ratios in the mixed SAMs were determined as listed in Table 3. Adsorbed amounts of **3**/Au and **5**/Au were calculated from the charge of the anodic peak of the boron−dipyrrin and the ferrocene moieties as 3.7 × 10^{-10} mol cm^{-2} and 1.9 × 10^{-10} mol cm^{-2},[16h] respectively (Figure 6a,b). These molecular areas of **3**/Au (= 45 Å^2

(29) (a) Imahori, H.; Hagiwara, K.; Akiyama, T.; Aoki, M.; Taniguchi, S.; Okada, T.; Shirakawa, M.; Sakata, Y. *Chem. Phys. Lett.* **1996**, *263*, 545. (b) Guldi, D. M.; Asmus, K.-D. *J. Am. Chem. Soc.* **1997**, *119*, 5744. (c) Kuciauskas, D.; Liddell, P. A.; Lin, S.; Stone, S. G.; Moore, A. L.; Moore, T. A.; Gust, D. *J. Phys. Chem. B* **2000**, *104*, 4307. (d) Imahori, H.; Tamaki, K.; Yamada, H.; Yamada, K.; Sakata, Y.; Nishimura, Y.; Yamazaki, I.; Fujitsuka, M.; Ito, O. *Carbon* **2000**, *38*, 1599. (e) Tkachenko, N. V.; Guenther, C.; Imahori, H.; Tamaki, K.; Sakata, Y.; Fukuzumi, S.; Lemmetyinen, H. *Chem. Phys. Lett.* **2000**, *326*, 344.

(30) Fujitsuka, M.; Ito, O.; Imahori, H.; Yamada, K.; Yamada, H.; Sakata, Y. *Chem. Lett.* **1999**, 721.

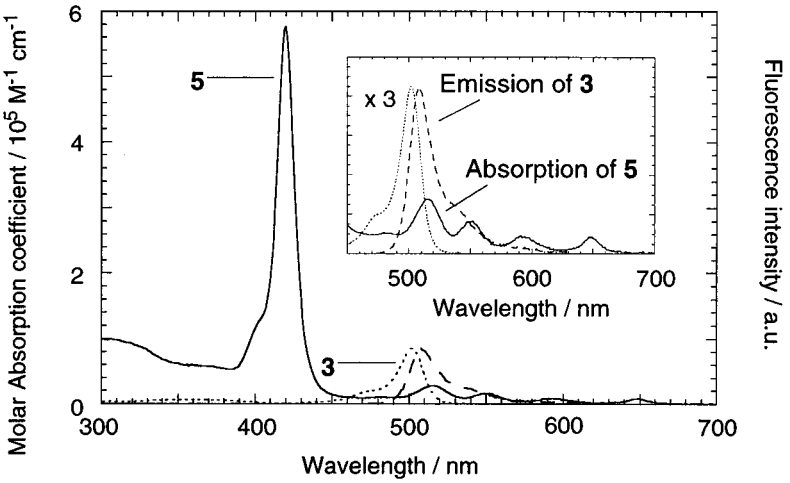

Figure 10. Absorption spectra of **3** (dotted line) and **5** (solid line) and fluorescence spectrum of **3** (dashed line, $\lambda_{ex} = 450$ nm) in CH_2Cl_2. Inset depicts the expanded spectra (×3) at 450−700 nm. The emission of **3** is normalized for comparison.

Table 3. Concentration Dependence of Quantum Yields in Au/**3**,**5**/MV^{2+}/Pt Cells

3:**5**[a] solution	**3**:**5**[b] mixed SAMs	surface coverage/10^{-10} mol cm^{-2},[b](absorbance)[c] **3**	**5**	quantum yield ϕ/%[d] 510 nm	430 nm
100:0	100:0	3.7 (0.015)	0	1.6± 0.3	
90:10	87:13	2.7 (0.011)	0.40 (0.0053)	8.9± 1.3	12± 2
75:25	71:29	2.3 (0.0094)	0.94 (0.014)	21± 3	19± 3
50:50	43:57	1.2 (0.0051)	1.6 (0.023)	45± 8	20± 3
25:75	37:63	1.0 (0.0042)	1.7 (0.030)	50± 8	21± 3
0:100	0:100	0	1.9 (0.039)		22± 3

[a] Molar ratio of **3**:**5** in CH_2Cl_2 solutions with the total concentration of 10 μM for formation of the mixed SAMs. [b] Molar ratio of **3**:**5** on the gold electrodes estimated from the electrochemical and absorption measurements.[16g,h] [c] Absorbance at the λ_{max} (**3**: 510 nm; **5**: ∼430 nm) on the gold surface. [d] $\phi = (i/e)/[I(1 - 10^{-A})]$, $I = (W\lambda)/(hc)$ where i is the photocurrent density, e is the elementary charge, I is number of photons per unit area and unit time, λ is the wavelength of light irradiation, A is absorbance of the adsorbed dyes at λ nm, W is light power irradiated at λ nm, c is the light velocity, and h is Planck's constant.

molecule^{-1}) and **5**/Au (= 87 Å^2 molecule^{-1}) agree well with the theoretical values of **3**/Au (45 Å^2 molecule^{-1}) and **5**/Au (86 Å^2 molecule^{-1}), which are calculated by assuming that the molecules are packed densely with a perpendicular orientation to the gold surface, respectively. Such an agreement indicates the formation of well-packed structures of **3** and **5** on the gold surface. Adsorbed amounts of **5** in the mixed SAMs (**3**,**5**/Au) were estimated from the charge of the anodic peak of the ferrocene moiety (Figure 6c). This method could not be applied to determine adsorbed amounts of **3** in **3**,**5**/Au because of the broadening and overlapping of the anodic peak of the boron−dipyrrin (Figure 6c), as in the cases of mixed SAMs of **1** and **2** as well as **3** and **4** on the gold surface. Instead, the adsorbed amounts of **3** in **3**,**5**/Au in Table 3 were calculated from absorption spectra of mixed SAMs of **3** and **5** on the gold surface, assuming that the molar absorption coefficient of **3** in the mixed SAMs of **3** and **5** is the same as that of **3**/Au (**3**: 4.1 × 10^7 mol^{-1} cm^2 ($\lambda_{max} = 510$ nm)). The ratios of **3**:**5** in **3**,**5**/Au are comparable to those in CH_2Cl_2 except for the case of the **3**:**5** ratio of 25:75 in solution where the corresponding ratio of **5** in **3**,**5**/Au (37:63) becomes somewhat smaller (Table 3). In contrast to the cases of **1**,**2**/Au and **3**,**4**/Au (vide supra), no significant preference of the adsorption of **3** over **5** on the gold surface is observed, indicating that $\pi-\pi$ interaction of the boron−dipyrrin moieties is similar to that of **5** which contains both the porphyrin and fullerene moieties.

The photoelectrochemical measurements were performed using the mixed SAMs of **3** and **5** on the gold electrodes in a three electrode system, denoted as Au/**3**,**5**/MV^{2+}/Pt cell, under the optimized conditions described above [electrolyte solution: O_2-saturated 0.1 M Na_2SO_4 solution containing 30 mM methyl viologen (MV^{2+}) as an electron carrier; input power: 380 μW cm^{-2}; applied potential: −200 mV vs Ag/AgCl].[16g,h,27,31,32] Figure 11 displays the action spectrum of Au/**3**,**5** (50:50)/MV^{2+}/Pt cell and absorption spectrum of **3**,**5** (50:50)/Au together with action spectrum of Au/**3** (50:50)/MV^{2+}/Pt cell. The Au/**3**,**5** (50:50)/MV^{2+}/Pt cell shows cathodic photoelectrochemical response from both the triad (**5**) (430 nm) and the boron−dipyrrin (**3**) units (510 nm), which agree with the absorption of **3**,**5** (50:50)/Au. It should be emphasized that the photocurrent generation efficiency of Au/**3**,**5** (50:50)/MV^{2+}/Pt cell at 510 nm is much larger than that of Au/**3**/MV^{2+}/Pt cell at 510 nm (Figure 11). The quantum yields determined were 45± 8% (510 nm) and 20 ± 3% (430 nm) for Au/**3**,**5** (50:50)/MV^{2+}/Pt cell and 1.6 ± 0.3% (510 nm) for Au/**3**/MV^{2+}/Pt cell. The quantum yield (45 ± 8% at 510 nm) of Au/**3**,**5**(50:50)/MV^{2+}/Pt cell is 28 times higher than that of Au/**3**/MV^{2+}/Pt cell (1.6 ± 0.3% at 510 nm) (Table 3).

The quantum yield of the Au/**3**,**5**/MV^{2+}/Pt cell determined based on the absorption of the porphyrin and the antenna molecules at 430 and 510 nm increases with an increase in the content of **5** in the SAMs. The EN efficiency from ^{1}B* in **3** to P in **5** may also increases with an increase in the content of **5** in the SAMs to reach the maximum values of the quantum yield

(31) The cathodic photocurrent in Au/**5**/Pt cell decreased (∼20%) by Ar bubbling into the solution, compared with that under the air-saturated conditions.[16h] On the other hand, intensity of the photocurrent increased (∼10%) by successive oxygen bubbling, and then recovered to the state under the Ar-saturated conditions by the following Ar bubbling into the solution.[16h] Thus, the results indicate that $C_{60}^{\bullet-}$ gives an electron to O_2 to produce $O_2^{\bullet-}$.

(32) When methyl viologen (MV^{2+}) was employed as an electron carrier in Au/**5**/Pt cell, the photocurrents increased with an increase of the MV^{2+} concentration under the Ar- or O_2-saturated conditions, implying that MV^{2+} also accepts an electron from $C_{60}^{\bullet-}$ to generate $MV^{\bullet+}$.[16h] This is supported by the fact that Fc^+−zincporphyrin (ZnP)-$C_{60}^{\bullet-}$ ion pair in benzonitrile reveals an intermolecular electron transfer from $C_{60}^{\bullet-}$ to large excess hexyl viologen perchlorate (HV^{2+}), which is similar to MV^{2+} in the first reduction potential, to produce the $HV^{\bullet+}$ in the transient spectra. As the concentration of MV^{2+} increased under the O_2-saturated conditions, the cathodic photocurrent increased by ∼20−30% and became saturated at around 30 mM MV^{2+}.[16h] Thus, all the photocurrent measurements in the present studies were performed under the optimized conditions (vide supra).

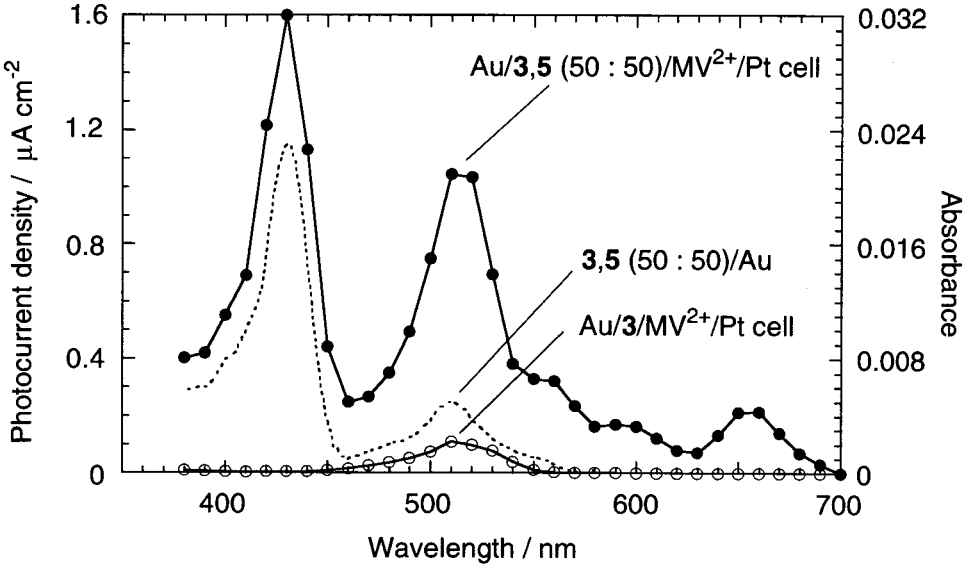

Figure 11. Action spectra of Au/**3**,**5** (50:50)/MV^{2+}/Pt cell (solid line with solid circles) and Au/**3**/MV^{2+}/Pt cell (solid line with open circles), and the absorption spectrum (dotted line) of a mixed SAM of **3** and **5** on the gold surface (**3**,**5** (50:50)/Au) from the CH_2Cl_2 solution with a molar ratio of 50:50; electrolyte solution: O_2-saturated 0.1 M Na_2SO_4 solution containing 30 mM methyl viologen (MV^{2+}) as an electron carrier; input power: 380 μW cm^{-2}; applied potential: −200 mV vs Ag/AgCl (saturated KCl)).

of 21 ± 3% (430 nm) and 50 ± 8% (510 nm) at the **3**:**5** ratio of 37:63 (Au/**3**,**5** (25:75)/MV^{2+}/Pt cell) (Table 3).[33] The incident photon-to-current efficiency (IPCE) of the Au/**3**,**5** (25:75)/MV^{2+}/Pt cell at 510 and 430 nm was also determined as 0.6% and 1.6%, respectively.[34] Formation of the CS state ($Fc^+-P-C_{60}^{\bullet-}$) in **5** following the EN and ET steps in Scheme 4 has been well established by the time-resolved transient absorption studies of the triad molecule **5** together with the fluorescence lifetime measurements,[16g,h] although the small absorbance of the present system has precluded the direct detection of the CS state within the SAMs. The quantum yield (50 ± 8%) at 510 nm is much higher than the value (20−25%) for the Au/**5**/MV^{2+}/Pt cell without **3**[16h] and this is the highest value ever reported for photocurrent generation at monolayer-modified metal electrodes and across artificial membranes using donor−acceptor linked molecules.[7−9,14−18] The coexistence of **3** as an antenna molecule in the Au/**3**,**5**/MV^{2+}/Pt system has enabled the utilization of the longer wavelength (510 nm) more efficiently as compared to the system without **3**. It should be noted here that the quantum yields of the Au/**3**,**5** (75:25, 50:50, 25:75)/MV^{2+}/Pt cell at 510 nm are higher than those at 430 nm. The fluorescence lifetime measurements of porphyrin SAMs on the gold surface indicate that $^1P^*$ is strongly quenched by the gold surface through EN.[16g,h] Thus, the higher quantum yields at 510 nm may result from the difference in quenching efficiency of S_1 and S_2 states of the porphyrin in **5** by the gold electrode.

In summary, the present system (i.e., mixed SAMs of boron−dipyrrin and ferrocene−porphyrin−fullerene triad) provides the first example of an artificial photosynthetic system, which not only mimics photoinduced EN and multistep ET in photosynthesis, but also act as an efficient light-to-current converter in molecular devices, accomplishing the highest quantum yield (50 ± 8%) ever reported in the related artificial photosynthetic systems. Although the IPCE value (1−2%) still remains low, further improvement may be possible by choosing chromophores which can absorb visible light more extensively and intensively.

(33) The emission of **3**,**5**/Au was too weak to be detected because of the efficient quenching of $^1P^*$ by an ET from $^1P^*$ to C_{60}, in addition to the $^1P^*$ quenching by the gold surface (Scheme 4).[16g,h,28]

(34) The low IPCE values result from the poor absorbance of the monolayers (absorbance = (4−40) × 10^{-3}).

Experimental Section

General. ^1H NMR spectra were measured on a JEOL EX-270. FAB mass spectra were obtained on a JEOL JMS-DX300. MALDI TOF mass spectra were measured on a Kratos Compact MALDI I (Shimadzu). UV−visible spectra in solutions were obtained on a Shimadzu UV3000 spectrometer, while those on gold substrates (Au/glass) were recorded on a Hitachi U-3500 spectrometer in transmission mode. Fluorescence spectra in solutions and on the gold substrate (Au/mica) were taken using a SPEX FluoroMAX-2 fluorometer and corrected.

Materials. All solvents and chemicals were of reagent grade quality, purchased commercially and used without further purification unless otherwise noted. Tetrabutylammonium hexafluorophosphate used as a supporting electrolyte for the electrochemical measurements was obtained from Tokyo Kasei Organic Chemicals. THF was purchased from Wako Pure Chemical Ind., Ltd., and purified by successive distillation over calcium hydride. Dichloromethane was refluxed and distilled from P_2O_5. Thin-layer chromatography (TLC) and flash column chromatography were performed with Art. 5554 DC-Alufolien Kiselgel 60 F_{254} (Merck), and Fujisilicia BW300, respectively.

Synthesis of Boron−Dipyrrin Thiol and Pyrene Disulfide. 8. 2,4-Dimethylpyrrole (2.16 mL, 21.1 mmol) and 4-nitrobenzaldehyde (1.87 g, 12.4 mmol) were added to CH_2Cl_2 (800 mL) in a 1 L round-bottom flask. The mixture was bubbled with N_2, and trifluoroacetic acid (0.19 mL, 2.47 mmol) was added and then stirred for 1.5 h. The resulting solution was washed with 0.1 M NaOH (200 mL) and then water (200 mL), dried over anhydrous Na_2SO_4, and filtered, and the solvent was evaporated on a rotary evaporator. The resultant product was used immediately. The product was redissolved in toluene (50 mL), and *p*-chloranil (2.73 g, 11.1 mmol) was added to the mixture. After the mixture stirred for 10 min, triethylamine (8 mL), and born trifluoride etherate (7 mL) were added. The mixture was stirred for 1.5 h, poured into water, and extracted with toluene. The toluene solution was extracted three times with 100 mL portions of water, and the solvent was evaporated on a rotary evaporator. The residue was redissolved in chloroform and applied to a silica gel flash column chromatography. Elution with 67% $CHCl_3$ in hexane v/v yielded 461 mg of **8**, 10%; ^1H NMR (270 MHz, $CDCl_3$) δ 8.38 (d, J = 9 Hz, 2H), 7.53 (d, J = 9 Hz, 2H), 6.02 (s, 2H), 2.56 (s, 6H), 1.36 (s, 6H); FAB-MS *m*/*z* 370 ($M + H^+$).

9. A solution of **8** (250 mg, 0.678 mmol) in THF (40 mL) was hydrogenated over 5% Pd on charcoal (250 mg) at room temperature and atmospheric pressure until TLC analysis indicated complete reduction of **8**. The catalyst was removed by filtration, and the filtrate was concentrated under vacuum. Flash column chromatography on silica

gel with toluene as an eluent yielded 91.1 mg of **9**, 40%; ^{1}H NMR (270 MHz, $CDCl_3$) δ 7.00 (d, J = 9 Hz, 2H), 6.77 (d, J = 9 Hz, 2H), 5.96 (s, 2H), 3.48 (br s, 2H), 2.54 (s, 6H), 1.49 (s, 6H); FAB-MS m/z 340 ($M + H^+$).

10. To a stirred solution of 2-chloro-4,6-dimethoxy-1,3,5-triazine (CDMT) (840 mg, 4.8 mmol), 12-bromododecanoic acid (1.12 g, 4 mmol) in THF (30 mL), *N*-methylmorpholine (0.53 mL, 4.8 mmol) was added dropwise at 0 °C, and stirring was continued at 0 °C for 5 h. To the crude solution, **9** (120 mg, 0.354 mmol) was added at 0 °C. Stirring continued for 16 h at room temperature, and the reaction mixture was evaporated to dryness in vacuo. Flash column chromatography on silica gel with toluene as the eluent yielded 176 mg of **10**, 83%; ^{1}H NMR (270 MHz, $CDCl_3$) δ 7.68 (d, J = 9 Hz, 2H), 7.24 (br.s, 1H), 7.22 (d, J = 9 Hz, 2H), 5.97 (s, 2H), 3.41 (t, J = 7 Hz, 2H), 2.55 (s, 6H), 2.39 (t, J = 7 Hz, 2H), 1.88 (quint, J = 7 Hz, 2H), 1.76 (quint, J = 7 Hz, 2H), 1.42 (s, 6H), 1.2−1.5 (m, 14H); FAB-MS m/z 601 ($M + H^+$).

11. A solution of **10** (85.0 mg, 0.142 mmol) and potassium thioacetate (51 mg, 0.45 mmol) in ethanol−THF (1:1 = v/v, 10 mL) was heated to reflux for 2 h. The solvent was then removed under a reduced pressure. Flash column chromatography on silica gel with toluene/ethyl acetate (19:1 = v/v) as an eluent yielded 74.6 mg of **11**, 88%; ^{1}H NMR (270 MHz, $CDCl_3$) δ 7.69 (d, J = 9 Hz, 2H), 7.18 (d, J = 9 Hz, 2H), 7.15 (br.s, 1H), 5.97 (s, 2H), 2.86 (t, J = 7 Hz, 2H), 2.54 (s, 6H), 2.37 (t, J = 7 Hz, 2H), 2.32 (s, 3H), 1.73 (quint, J = 7 Hz, 2H), 1.56 (quint, J = 7 Hz, 2H), 1.42 (s, 6H), 1.2−1.5 (m, 14H); FAB-MS m/z 596 ($M + H^+$).

3. A solution of **11** (68.0 mg, 0.114 mmol) and KOH (10 mg) in methanol−THF (1:1 = v/v, 20 mL) was refluxed under a nitrogen atmosphere in the dark for 5 min. After cooling, the mixture was poured onto 20 mL of brine and extracted with toluene. The extract was dried over anhydrous Na_2SO_4, and the solvent was removed under reduced pressure. Flash column chromatography on silica gel with toluene/ethyl acetate (19:1 = v/v) as an eluent yielded 55.4 mg of **3**, 88%; ^{1}H NMR (270 MHz, $CDCl_3$) δ 7.68 (d, J = 9 Hz, 2H), 7.51 (br.s, 1H), 7.20 (d, J = 9 Hz, 2H), 5.97 (s, 2H), 2.52 (s, 6H), 2.50 (q, J = 7 Hz, 2H), 2.37 (t, J = 7 Hz, 2H), 1.72 (quint, J = 7 Hz, 2H), 1.61 (quint, J = 7 Hz, 2H), 1.42 (s, 6H), 1.2−1.5 (m, 14H); FAB-MS m/z 554 ($M + H^+$); UV−vis (CH_2Cl_2) λ_{max} (log ϵ) 249 (4.43), 307 (3.60), 358 (2.55), 502 (4.93).

6. This compound was synthesized from 1-aminopyrene and 12-bromododecanoic acid by the same method as described for **10**. **6** as a white solid (29% yield); ^{1}H NMR (270 MHz, $CDCl_3$) δ 7.7−8.3 (m, 10H), 3.39 (t, J = 8 Hz, 2H), 2.54 (t, J = 8 Hz, 2H), 1.0−2.0 (m, 18H); MALDI-TOF m/z 478, 480 ($M + H^+$).

7. This compound was synthesized from **6** by the same method as described for **11**. **7** as a white solid (52% yield); ^{1}H NMR (270 MHz, $CDCl_3$) δ 8.39 (d, J = 8 Hz, 1H), 7.9−8.3 (m, 8H), 7.80 (br.s, 1H), 2.85 (t, J = 8 Hz, 2H), 2.60 (t, J = 8 Hz, 2H), 2.31 (s, 3H), 1.89 (t, J = 8 Hz, 2H), 1.0−1.7 (m, 16H); MALDI-TOF m/z 474 ($M + H^+$).

1. This compound was synthesized from **7** by the same method as described for **3**. **1** as a white solid (42% yield); ^{1}H NMR (270 MHz; $CDCl_3$) δ 7.7−8.3 (m, 20H), 2.68 (t, J = 8 Hz, 4H), 2.58 (t, J = 8 Hz, 4H), 2.0−1.0 (m, 36H); MALDI-TOF m/z 862 ($M + H^+$).

4. This compound was synthesized by following the similar procedures as described previously.[16g] **4** as a red−black solid (46% yield); ^{1}H NMR (270 MHz, $CDCl_3$) δ 8.90 (s, 4H), 8.89 (d, J = 5 Hz, 2H), 8.86 (d, J = 5 Hz, 2H), 8.18 (d, J = 8 Hz, 2H), 8.08 (d, J = 2 Hz, 4H), 8.07 (d, J = 2 Hz, 2H), 7.91 (d, J = 8 Hz, 2H), 7.78 (t, J = 2 Hz, 2H), 7.77 (t, J = 2 Hz, 1H), 7.49 (br.s, 1H), 2.55 (t, J = 8 Hz, 2H), 2.54 (q, J = 8 Hz, 2H), 1.2−1.9 (m, 19H); MALDI-TOF m/z 1168 ($M + H^+$).

Preparation of Modified-Gold Electrodes. The gold electrodes (Au(111)) were prepared by a vacuum-deposition technique with gold (1000 Å) onto fresh mica (roughness factor R = 1.1) or with gold (200 Å) onto transparent glass slide (R = 1.5) for the measurements of absorption spectra in transmission mode.[16g,h] For the time-resolved fluorescence measurements, gold substrates were prepared by a vacuum deposition technique with titanium (50−100 Å) and gold (200−1000 Å) in a sequence onto Si (100) wafer (Sumitomo Sitix Corp.). The gold electrodes on mica were annealed with hydrogen flame for 30 s immediately prior to immersion into the solutions. Monolayers of mixtures of **1**,**2**/Au (or **3**,**4**/Au or **3**,**5**/Au) were formed by the coadsorption onto Au(111)mica substrates. The coadsorption onto the gold surface was carried out from CH_2Cl_2 solutions containing **1** and **2** (or (**3** and **4**) or (**3** and **5**)) with the total concentration of 10 μM for 20 h to complete the mixed SAM formation. After soaking, the gold substrate was washed well with CH_2Cl_2 and dried with a stream of argon.

Estimate of Surface Coverage. All electrochemical studies were performed on a Bioanalytical Systems, Inc. CV-50W voltammetric analyzer using a standard three-electrode cell with a modified Au working electrode (0.48 cm^2), a platinum wire counter electrode, and a Ag/AgCl (saturated KCl) reference electrode. The adsorbed amount of **5** in **3**,**5**/Au was determined from the charge of the anodic peak of the ferrocene. The adsorbed amounts of **1** and **2** in **1**,**2**/Au, **3** and **4** in **3**,**4**/Au, and **3** in **3**,**5**/Au were estimated from the absorbance at the gold surface, assuming that the molar absorption coefficients of **1**−**4** in the mixed SAMs are the same as those of **1**/Au, **2**/Au, **3**/Au, and **4**/Au.

Photoelectrochemical Measurements. Photoelectrochemical measurements were performed in a one-compartment Pyrex UV cell (5 mL).[16g,h] The cell was illuminated with monochromatic excitation light through a monochromator (Ritsu MC-10N) by a 500 W xenon lamp (Ushio XB-50101AA-A) on the SAM of 0.48 cm^2. The photocurrent was measured in a three-electrode arrangement (Bioanalytical Systems, Inc., CV-50W), a modified gold working electrode, a platinum wire counter electrode (the distance between the electrodes is 0.3 mm), and a Ag/AgCl (saturated KCl) reference. The light intensity was monitored by an optical power meter (Anritsu ML9002A) and corrected.

Quantum efficiencies were calculated based on the number of photons absorbed by the chromophore on the gold electrodes at each wavelength using the input power (380 μW cm^{-2}), the photocurrent density, and the absorbance determined from the absorption spectrum on the gold electrode. The absorbance at each wavelength was converted into the net absorbance, including contribution of the reflection on the gold surface, using the reflectivity of the incident light (38.7% at 430 nm and 54.5% at 510 nm), and the roughness factor of the gold electrodes.

Fluorescence Lifetime Measurements. Fluorescence decays were measured by using a femtosecond pulse laser excitation and a single-photon counting system for fluorescence decay measurement. The laser system was a mode-locked Ti:Sa laser (Coherent, Mira 900) pumped by an argon ion laser (Coherent, Innova 300). The repetition rate of a laser pulse was 2.9 MHz with a pulse picker (Coherent, model 9200). The third harmonic generated by an ultrafast harmonic system (Inrad, model 5-050) was used as an excitation source. The excitation wavelength was set at 280 nm (or 261 nm) and temporal profiles of fluorescence decay and rise were recorded by using a microchannel plate photomultiplier (Hamamatsu R3809U). Full-width at half-maximum (fwhm) of the instrument response function was 36 ps where the time interval of the multichannel analyzer (CANBERRA, model 3501) was 2.6 ps in the channel number. The fluorescence decays were measured at 385 nm for the pyrene moiety and at 720 nm for the porphyrin moiety. Criteria for the best fit were the values of χ^2 and the Durbin-Watson parameters, obtained by nonlinear regression.[35]

Acknowledgment. This work was supported by COE and Grant-in-Aid for Scientific Research on Priority Area of Electrochemistry of Ordered Interfaces and Creation of Delocalized Electronic Systems from Ministry of Education, Science, Sports and Culture, Japan. H.I. thanks the Sumitomo Foundation for financial support.

JA002154K

(35) (a) Boens, N.; Tamai, N.; Yamazaki, I.; Yamazaki, T. *Photochem. Photobiol.* **1990**, *52*, 911. (b) Nishimura, Y.; Yasuda, A.; Speiser, S.; Yamazaki, I. *Chem. Phys. Lett.* **2000**, *323*, 117.